CEREBRAL VASCULAR ENHANCEMENT USING A WEIGHTED 3D SYMMETRY FILTER

Lingling Luo[1], *Yitian Zhao*[1*], *Jian Yang*[1], *Yalin Zheng*[2], *Siyuan Yang*[1], *Danni Ai*[1], *Yongtian Wang*[1]

[1]Beijing Engineering Research Center of Mixed Reality and Advanced Display, School of Optics and Electronics, Beijing Institute of Technology, Beijing, China.

[2]Department of Eye and Vision Science, University of Liverpool, Liverpool, UK

[*]E-mail: yitian.zhao@bit.edu.cn

ABSTRACT

The automated detection of cerebral vessels is of great importance in understanding of the diagnosis, treatment and mechanism of many brain vascular pathologies. However, automatic vessel detection from 3D angiography continues to be an open issue. In this paper we introduce a novel 3D symmetry filter that has excellent performance on enhancing vessels in magnetic resonance angiography (MRA). The proposed filter not only takes into account of local phase features estimated by using a quadrature filter so as to distinguish between lines and the edges, but also uses the weighted geometric mean of the blurred and shifted responses of the quadrature filter, which allows more tolerance in the position of the respective contours. As a result this filter can produce a strong response to the vascular features despite variations in scale, contrast, and bifurcations in images. Our results demonstrate its superior performance to other state-of-the-art methods.

Index Terms— cerebral, vascular, quadrature, symmetry, MRA, enhancement;

1. INTRODUCTION

Recent years the vessel segmentation methods for different types of medical images have been developed rapidly, as evidenced by extensive reviews, such as a general review on this topic [1], and a review on 3D vessel segmentation [2]. However, the segmentation of cerebral vessels is a relatively unexplored field, primarily due to the complex geometry involved, as well as problems posed by low image contrast and spatial resolution.

For the purposes of this paper, only cerebral vascular segmentation techniques will be reviewed, with the intention of providing readers with some insight into this problem domain: the review is thus by no means exhaustive in terms of automated analysis vessels. Manniesing et al. [3] reported a level set method for the segmentation of cerebral vessels from CT angiography (CTA). However, the proposed method is relatively time consuming for the segmentation. Hernandez et al. [4] proposed a method based on non-parametric geodesic active regions (GAR), and provided promising segmentation results of vasculature and aneurysm from 3D Rotational Angiography (3DRA) and Computed Tomography Angiography (CTA). Babin et al. [5] proposed a line-shaped profiling method with applications to cerebral vessels and arteriovenous malformations. Bogunovic et al. [6] improved the GAR and evaluated its potential and limitations in segmenting cerebral vessels with aneurysms from 3DRA and time of flight magnetic resonance angiography (TOF-MRA) images. Recently, Cetin and Unal [7] introduced a cylindrical flux-based higher order tensor for vessel segmentation, and evaluated it on both synthetic complex tubular structures and real cerebral vasculature in MRA datasets and coronary arteries from CTA volumes. On the other hand, various filtering-based methods have been adapted to enhance images of cerebral vasculature for the purpose of segmentation, such as Hessian matrix-based filters [8, 9, 10], local phase filters [11, 12, 13], flux-based [14, 15], or tensor-based filtering [7, 16], and various wavelet [17], and Gabor filters [18].

These aforementioned methods have yet to completely solve the problems posed by the high degree of anatomical variation across the population and varying scales of vessels within an image. Moreover, artifacts occurred during image acquisition, such as noise, poor contrast and low resolution, exacerbate these problems. As a result, it has proven very difficult to choose global appropriate parameters for a segmentation method that is available for different image data. In this paper we introduce a novel 3D symmetry filter for cerebral vascular enhancement. This paper makes three contributions. Firstly the proposed 3D filter overcomes the inherent problem of vessel enhancement in medical images. Secondly, the proposed filter can produce dimensionless measures of vesselness independent of the image illumination or contrast. As such universal solutions may have the potential to be approached to segment vessels for different types of image modalities. Thirdly the paper demonstrates its superiority to other contemporary methods on the segmentation of MRA images.

2. METHOD

In this section, we will present the details of the proposed 3D symmetry filter. First, we will introduce 3D quadrature filter

in general from which local phase information can be derived. Classic 3D symmetry filter is then derived based on the local phase information that can enhance tubular structures. A new weighted 3D symmetry filter is proposed by applying blurring and shifting operators to the standard 3D symmetry filter and combining responses from different scales and orientations.

2.1. 3D Quadrature filter

Quadrature filter is a well-established tool for extracting local structure information in images. It can distinguish the intrinsic information of features in an image such as local phase and energy. Local phase is invariant to changes in illumination and can be estimated by the Hilbert Transform under the concept of analytical signal [19].

The Hilbert Transform is defined over the whole spectrum of the signal. In other words, in order to enhance spatial localization and to avoid the effects of noise, the analysis of the signal must be undertaken over a narrow range of frequencies at different locations in the signal. Boukerroui et al. [20] suggested making use of a band-pass filter, and proposed in addition that the filter should be symmetric, or even (with constant phase, so as not to change the phase information of the original signal). The phase can be defined as:

$$\phi(x) = \arctan\Big(\frac{f_e(x) * f(x)}{f_o(x) * f(x)}\Big) = \arctan\Big(\frac{E(x)}{O(x)}\Big), \quad (1)$$

where $*$ denotes the convolution operator and $f_o(x)$ and $f_e(x)$ are the odd and even filter pair of a quadrature filter. A quadrature filter consists with even-symmetric $E(x)$ and odd-symmetric parts $O(x)$. The log-Gabor filter has been a common choice of quadrature filters [21, 12]. It can been seen that at edges, the odd-symmetric parts has the maximal response, while the even-symmetric is almost 0, the filter response is purely imaginary, and the filtered signal is strongly 'edge-like': while at lines odd-symmetric is almost 0 and even-symmetric has maximal response, the filter response is purely real, and leads to an 'line-like' signal. This suggests that edges align with the zero crossing of the real part of the phase map.

The extension of the quadrature filter to 3D is accomplished in this paper, by designing a 3D log-Gabor filter. The transfer function of the 3D log-Gabor filter in the frequency domain is defined as:

$$LG = \exp\left(-\frac{\log\Big(\frac{\omega(p)}{\omega_0}\Big)^2}{2\log\Big(\frac{k}{\omega_0}\Big)^2}\right) \times \exp\Big(-\frac{\alpha(p,\Phi_1,\Phi_2)^2}{2\tau_\alpha^2}\Big), \quad (2)$$

where the first and second term are the log-Gabor and Gaussian functions, respectively. The bandwidth of the filter in the radial direction is determined by a scaling factor k, and ω_0 is the center spatial frequency of the filter. p is a point in the frequency domain with $\omega(p) = \|p\|$. The azimuth (Φ_1) and elevation (Φ_2) are the angles between the directions of the filter. The position vector at point p in the frequency domain is given by $\alpha(p,\Phi_1,\Phi_2) = \arccos(p \times \frac{\nu}{\|p\|})$, where $\nu = (\cos\Phi_1\cos\Phi_2, \cos\Phi_1\sin\Phi_2, \sin\Phi_2)$ is a unit vector. τ_α is the standard deviation of the Gaussian function in the angular direction, which describes the angular selectivity of the filter.

2.2. 3D Symmetry filter

As suggested by Kovesi [22], an image symmetry measure can be used to identify that the response of the even filter dominates the response of the odd filter by taking the difference of their absolute values, and the symmetric responses of the filter in 3D domain can thus be determined:

$$\varrho(u,v,w) = \frac{\sum_{\theta=1}^{\Theta}\left(|E_\theta(u,v,w)| - |O_\theta(u,v,w)| - T\right)}{\sum_{\theta=1}^{\Theta}\sqrt{E_\theta^2(u,v,w) + O_\theta^2(u,v,w)} + \varepsilon}, \quad (3)$$

where the even and odd filters are defined as

$$E^n(u,v,w) = \text{real}(F^{-1}LG \times F(I(u,v,w))), \quad (4)$$

$$O^n(u,v,w) = \text{imag}(F^{-1}LG \times F(I(u,v,w))). \quad (5)$$

Here, E^n and O^n denote the responses of even symmetric and odd symmetric parts of a quadrature filter at scale n. F and F^{-1} denote the forward and inverse 3D Fourier Transforms, and $I(u,v,w)$ indicates the intensity value at location (u,v,w). In practice, multiple orientations (θ) are needed to capture structures at different directions, with the intention of achieving a rationally invariant response. ε was set to 0.001 (as was done in [23, 22]), and Θ indicates the total number of directions under consideration, which given as $\theta = \{\frac{\pi}{4}, \frac{\pi}{2}, \frac{3\pi}{4}, \pi\}$. The kernel size is 15×15. The constant ε is able to prevent division by zero in the case in which the signal is uniform and no filter response is obtained. T denotes the compensation term of the noise, which representing the noise alone in the signal could generate the maximum response: $T = \mu + \nu \times \sigma$. This factor can be obtained by combining the estimated influence of noise on each of the filters: μ is mean of the local energy distribution of noise, and the distribution of noise is expected to be Rayleigh. σ denotes the standard deviation of the local energy distribution of noise, and ν is a specified number that provide a balance between the vessels and background, and was set to 5.

2.3. Blurring and shifting

In order to allow for greater tolerance in the positions of the respective contours, blurring and shifting operations on the proposed filter responses are required. As inspired by [24], the blurring operation is taken by using a Gaussian function G_σ on the responses of the proposed filter. σ indicates the standard deviation of the quadrature filter that responds most strongly to edge features: it can be determined by $\sigma = \sigma_0 + \alpha\rho$, where σ_0 and α are constants, and ρ is the radius representing a linear function of the distance from the centre of the quadrature filter. The choice of the value ρ is related to the size and complexity of the local pattern.

Each blurred quadrature response will then be shifted respectively by a distance ρ_i in the direction opposite to ϕ_i. In Cartesian coordinates, the shift vector in question is

$(\Delta u_i, \Delta v_i, \Delta w_i)$, where $\Delta u_i = -\rho_i \cos\phi_i$, $\Delta v_i = -\rho_i \sin\phi_i$, and $\Delta w_i = -\rho_i \sin\phi_i$. Finally, the blurred and shifted response of the quadrature filter for each tuple $(\sigma_i, \rho_i, \phi_i)$ in set S is defined:

$$S_{\sigma_i,\rho_i,\phi_i}(u,v,w) = \max_{u',v',w'} \{\varrho_{\sigma_i}(u - \Delta u_i - u', v - \Delta v_i - v', w - \Delta w_i - w') G_{\sigma'}(u',v',w')\}. \quad (6)$$

The above process obtains the responses in different positions (ρ_i, ϕ_i) with respect to the filter centre. In consequence, the shift operation is able to assemble all the responses in the proposed filter centre. The response $\mathcal{R}(u,v,w)$ is the blurred and shifted response of the quadrature filter, which can be obtained by thresholding the responses:

$$\mathcal{R}(u,v,w) = \left| \left(\prod_{i=1}^{|S|} (S_{\sigma_i,\rho_i,\phi_i}(u,v,w)^{\omega_i}) \right)^{\tau} \right|_t, \quad (7)$$

$$\tau = \frac{1}{\sum_{i=1}^{|S|} \omega_i}, \quad \omega_i = \exp(-\frac{\rho_i^2}{2\overline{\sigma}^2}), \quad \overline{\sigma} = \frac{1}{3} \max_{i \in \{1 \cdots |S|\}} \{\rho_i\}$$

where $|\cdot|_t$ aims to threshold the response at a fraction $t (0 \leq t \leq 1)$ of the maximum responses. The multiplication operator is applied to force only in the case that all the afferent blurred and shifted responses must be greater than zero to achieve a response. In practice, the weight achieves the maximum value $\omega = 1$ when $\rho = 0$, while reaches the minimum value $\omega = 0.5$ if $\rho = \rho_{\max}$.

Finally, the responses from different scales are combined. The response of the proposed 3D filter at each scale is weighted by the βth power of the magnitude of the filter response at that scale n, and the weighted difference is then normalized by the sum of the magnitude of the filter response vectors over all scales:

$$\mathcal{R} = \frac{\sum_{n=1}^{N} \mathcal{R}_n |\mathcal{R}_n|^{\beta}}{\sum_{n=1}^{N} |\mathcal{R}_n|^{\beta}} \quad (8)$$

3. EXPERIMENTS AND RESULTS

We evaluated the proposed enhancement method against a publicly available dataset - MIDAS [25] with 50 ToF MRA images. These images were captured by a 3T unit under standardized protocols, with voxel size of $0.5 \times 0.5 \times 0.8\ mm^3$, and reconstructed with $448 \times 448 \times 128$ matrix.

In order to quantitatively evaluate the performance of the proposed method, two types of reference standard, manual and semi-manual annotations, were used in this work. ***Manual annotation***: As in the annotations of the Grand Challenge of VESsel SEgmentation in Lung (VESSEL12) [26], we asked two graders to annotate four axial slices of each case. 360 landmarks were labeled in each case, of which 220 and 140 were annotations on vascular and non-vascular regions, respectively. The points located at the vessel bifurcations, bent vessels, or regions where the proposed method was expected to differ most clearly are annotated as vascular landmarks. A consensus between two of the graders was used as the final reference standard. Based on the diameters of vessels, the slices which contained a high proportion of Circle of Willis (CoW), large, medium, and small vessels were selected for annotation. Fig. 2 illustrates manual annotation imposed on 2D, 3D and maximum intensity projection (MIP) images. ***Semi-manual annotation:*** Bogunovic et al. [6] employed an open source tool kit - TubeTK [27] to generate an almost-manual annotation of the same dataset: by tracing the centerline of the vessel, and the vessel surface was extracted using the geodesic active contour method [28], as shown as Fig. 2(b). It should be noted that, this annotation concentrates on the vessels located in the region of the Circle of Willis only: accordingly we use this annotation to validate the performance of the proposed method on the CoW.

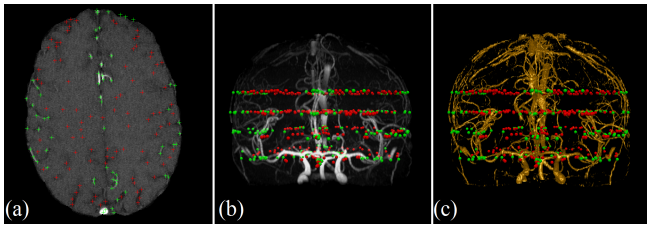

Fig. 1. Manual annotations. (a) Manually annotated landmarks displayed on one axial slice. (b) Landmarks displayed on MIP. (c) Landmarks displayed on proposed segmentation result. Red: non-vascular region; Green: vascular region.

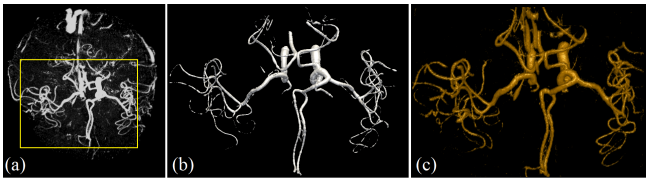

Fig. 2. Semi-manual annotations. (a) MIP view of a sample MRA: the selected region indicates the region of the CoW. (b) Semi-manual annotation on the CoW by the method of Bogunovic et al.[6]. (c) The performance of our method.

The top row of Fig. 3 shows a slice of an MRA scan, and the results after applying three state-of-the-art medical image enhancement functions: the *Frangi's Vesselness Filter (FVF)* [8], the *Isotropic Undecimated Wavelet Filter (IUWF)* [17], and the *3D Local Phase Filter (LPF)* [11], as well as the proposed method. The default parameters were used in the experiments. Overall, all methods demonstrate similar performance on the large vessels. However, for accurate observation of small vessels, the proposed method provides relatively stronger responses than other enhancement methods, and this is confirmed by the middle row of Fig. 4 - the corresponding MIP results. In contrast, the proposed method provides brighter results as compared to other

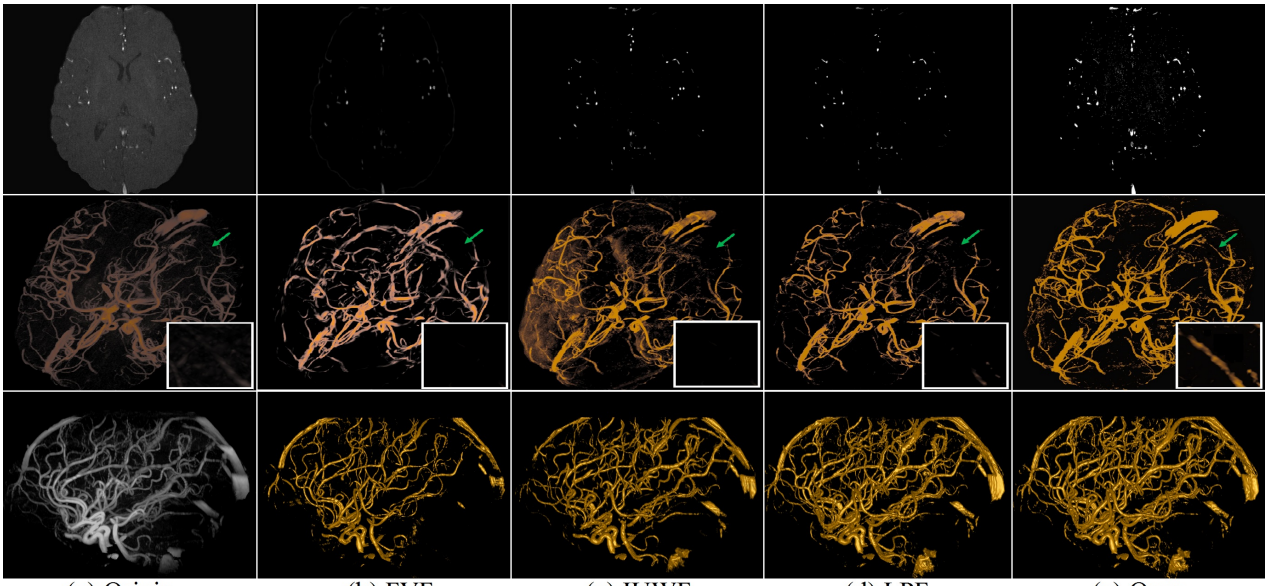

(a) Origin (b) FVF (c) IUWF (d) LPF (e) Ours

Fig. 3. Performances of different vessel detection methods on both 2D and 3D. From top to bottom: enhancement results on one axial slice; enhanced result are visualized in 3D by MIP; vascular segmentation results.

Table 1. Segmentation results obtained using different vascular enhancement methods.

Methods	TP	FN	FP	OM
FVF	91.43%	5.24%	7.48%	91.41%
IUWF	93.87%	5.02%	7.02%	92.44%
LPF	94.12%	4.83%	6.91%	93.89%
Proposed	95.78%	4.42%	6.62%	95.01%

Table 2. Segmentation results obtained on the Circle of Willis by using different cerebral vascular segmentation methods.

Methods	TP	FN	FP	OM
HOOI	94.54%	5.46%	7.45%	92.86%
RAnk-1	95.43%	4.57%	6.57%	94.78%
ITM	93.07%	6.93%	9.82%	91.74%
Proposed	96.24%	3.87%	5.91%	95.53%

methods, and it demonstrates better performance in enhancing the small vessel indicated by the green arrow. The bottom row of Fig. 3 shows the segmentation results obtained using different enhancement methods at the optimal threshold: it reveals that our method is able to detect more small vessels.

In addition to visual inspection of the results, objective evaluation was also undertaken by comparing the segmentation results from different methods. Quantitatively evaluation results are reported in Table 1 in terms of True Positives (TP), False Negatives (FN), False Positives (FP), and Overlap Measure (OM). The optimal threshold values (FVF: 0.75, IUWF: 0.75, LPF: 0.80, proposed: 0.80) were determined at the highest overlapping measure (OM). Overall, the proposed method achieves the best scores in terms of all the metrics, with TP=95.78%, FN=4.42%, FP=6.62%, and OM=95.01%. In addition, evaluations of performance on segmenting the CoW were performed based on semi-manual annotation provided by Bogunovic et al. [6], and compared with three state-of-the-art cerebral vessel segmentation methods: *Higher Order Orthogonal Iteration (HOOT)* [15], *Finding Rank-1 Approximation (RAnk-1 Approx)* [16], and *Intensity-based Tensor Model (ITM)* [7]. The results show that our method achieves the best performance, with TP=96.23%, FN=3.87%, FP=5.91%, and OM=95.53%.

4. CONCLUSIONS

In this paper, we have presented a new weighted 3D symmetry filtering technique for cerebral vasculature enhancement. The proposed filter exploits the advantages of local phase as estimated by a 3D quadrature filter, and by the geometric mean of the blurred and shifted quadrature filter responses, as thus to allow more tolerance in the position of the respective contours. Visual inspection and quantitative evaluations on the MIDAS dataset showed that, compared to other established methods, the proposed filter obtains better vascular detection performance. The evaluation results in Table 1 and Table 2 demonstrate that the superiority of our model when compared with other state-of-the-art methods. It is worth noting that in Fig. 3, the results of the proposed method on segmenting the CoW is very close to that of the semi-manual method, and even demonstrates better performance on relatively low intensity regions. This is because GAR responds only weakly to poor intensity regions. It is our intention in our future work to evaluate the segmentation performance on the CoW, large, medium and small vessels individually.

5. ACKNOWLEDGEMENT

The authors thank Dr. Hrvoje Bogunovic for sharing the manual segmentation results of 50 subjects in the MIDAS MRA dataset. This work was supported by National Science Foundation Program of China (61601029,61602322).

6. REFERENCES

[1] M. Fraz, P. Remagnino, A. Hoppe, B. Uyyanonvara, A. R. Rudnicka, C. G. Owen, and S. A. Barman, "Blood vessel segmentation methodologies in retinal images - a survey," *Comput. Meth. Prog. Bio.*, vol. 108, pp. 407–433, 2012.

[2] D. Lesagea and G. Funka-Leaa, "A review of 3D vessel lumen segmentation techniques: Models, features and extraction schemes," *Med. Image Anal.*, vol. 13, pp. 819–845, 2009.

[3] R. Manniesing, M. Viergever, A. Lugt, and W. Niessen, "Cerebral arteries: Fully automated segmentation from CT angiographya feasibility study," *Radiology*, vol. 247, pp. 247–846, 2008.

[4] M. Hernandez and A. F. Frangi, "Non-parametric geodesic active regions: Method and evaluation for cerebral aneurysms segmentation in 3DRA and CTA," *Med. Image Anal.*, vol. 11, no. 3, pp. 224–241, 2007.

[5] D. Babin, A. Pizurica, J. Vylder, E. Vansteenkiste, and W. Philips, "Brain blood vessel segmentation using line-shaped profiles," *Phy. Med. Bio.*, vol. 58, pp. 8041–8061, 2013.

[6] H. Bogunovic, J. Pozo, and A. Frangi, "Automated segmentation of cerebral vasculature with aneurysms in 3DRA and TOF-MRA using geodesic active regions: An evaluation study," *Med. Phys.*, vol. 38, pp. 210–222, 2011.

[7] S. Cetin and G. Unal, "A higher-order tensor vessel tractography for segmentation of vascular structures," *IEEE Trans. Med. Imag.*, vol. 34, no. 10, pp. 2172–2185, 2015.

[8] Alejandro F. Frangi, Wiro J. Niessen, Koen L. Vincken, and Max Viergever Viergever, "Multiscale vessel enhancement filtering," in *Med. Image Comput. Comput. Assist. Interv.*, 1998, vol. 1496, pp. 130–137.

[9] Y. Sato, C. Westin, A. Bhalerao, S. Nakajima, N. Shiraga, and S. Tamura, "Tissue classification based on 3D local intensity structures for volume rendering," *IEEE Trans. Vis. Comput. Graph.*, vol. 6, no. 2, pp. 160–180, 2000.

[10] T. Jerman, F. Penus, B. Likar, and Z. Spiclin, "Enhancement of vascular structures in 3D and 2D angiographic images," *IEEE Trans. Med. Imag.*, vol. 35, no. 9, pp. 2107–2118, 2016.

[11] G. Lathen, J. Jonasson, and M. Borga, "Blood vessel segmentation using multi-scale quadrature filtering," *Pattern Recogn. Lett.*, vol. 31, pp. 762–767, 2010.

[12] Y. Zhao, Y. Liu, X. Wu, S.P. Harding, and Y. Zheng, "Retinal vessel segmentation: An efficient graph cut approach with retinex and local phase," *PLoS ONE*, vol. 10, pp. e0122332, 2015.

[13] Y. Zhao, L. Rada, K. Chen, S. P. Harding, and Y. Zheng, "Automated vessel segmentation using infinite perimeter active contour model with hybrid region information with application to retinal images," *IEEE Trans. Med. Imag.*, vol. 34, pp. 1797–1807, 2015.

[14] D. Lesage, E. D. Angelini, I. Bloch, and G. Funka-Lea, "Bayesian maximal paths for coronary artery segmentation from 3D CT angiograms," in *Med. Image Comput. Comput. Assist. Interv.*, 2009, pp. 222–229.

[15] S. Cetin, A. Demir, A. Yezzi, M. Degertekin, and G. Unal, "Vessel tractography using an intensity based tensor model with branch detection," *IEEE Trans. Med. Imag.*, vol. 32, no. 2, pp. 348–363, 2013.

[16] T. Schultz and H. Seidel, "Estimating crossing fibers: A tensor decomposition approach," *IEEE Trans. Vis. Comput. Graph.*, vol. 14, pp. 1635–1642, 2008.

[17] P. Bankhead, J. McGeown, and T. Curtis, "Fast retinal vessel detection and measurement using wavelets and edge location refinement," *PLoS ONE*, vol. 7, pp. e32435, 2009.

[18] J. Soares and M. Cree, "Retinal vessel segmentation using the 2D Gabor wavelet and supervised classification," *IEEE Trans. Med. Imag.*, vol. 25, pp. 1214–1222, 2006.

[19] M. Felsberg and G. Sommer, "The monogenic signal," *IEEE Trans. Signal Process.*, vol. 49, pp. 3136–3144, 2001.

[20] D. Boukerroui, J. Noble, and M. Brady, "On the choice of band-pass quadrature filters," *J. Math. Imaging Vis.*, vol. 21, pp. 53–80, 2004.

[21] I. Hacihaliloglu, A. Rasoulian, P. Abolmaesumi, and R. Rohling, "Local phase tensor features for 3d ultrasound to statistical shape+pose spine model registration," *IEEE Trans. Med. Imag.*, vol. 33, pp. 2167–2179, 2014.

[22] P. Kovesi, "Symmetry and asymmetry from local phase," in *Tenth Australian Joint Converence on Artificial Intelligence*, 1997, pp. 2–4.

[23] I. Hacihaliloglu, A. Rasoulian, P. Abolmaesumi, and R. Rohling, "Automatic bone localization and fracture detection from volumetric ultrasound images using 3d local phase features," *Ultrasound in Med. and Bio.*, vol. 38, pp. 128144, 2012.

[24] G. Azzopardi, N. Strisciuglio, M. Vento, and N. Petkov, "Trainable COSFIRE filters for vessel delineation with application to retinal images," *Med. Image Anal.*, vol. 19, pp. 46–57, 2015.

[25] MIDAS, "http://insight-journal.org/midas/community/view/21/," .

[26] R. Rudyanto, S. Kerkstra, and et al., "Comparing algorithms for automated vessel segmentation in computed tomography scans of the lung: the VESSEL12 study," *Med. Image Anal.*, vol. 18, pp. 1217–1232, 2014.

[27] D. Pace, "Tubetk: An open-source toolkit of algorithms operating on images of tubes," in *Int. Congr. Exhibit. CARS.*, 2012, vol. 7, pp. S79–S80.

[28] H. Bogunovic, J. Pozo, and A. Frangi, "Anatomical labeling of the circle of willis using maximum a posteriori probability estimation," *IEEE Trans. Med. Imag.*, vol. 32, no. 9, pp. 1587–1599, 2013.